Research Article

Formation of nanodimensional structures in precipitated hydroxyapatite by fluorine substitution

Ekaterina A. Bogdanova[1] · Vladimir M. Skachkov[1] · Irina S. Medyankina[1] · Hartmuth Schröttner[2] · Nail A. Sabirzyanov[1] · Andrey A. Rempel[3]

Abstract

Hydroxyapatite $Ca_{10}(PO_4)_6(OH)_2$ is a bioactive compound, which is of great interest for medical application as a component of artificial bones and implants. The modification of its composition via anion and cation substitution can strongly affect its properties due to the formation of nanosized particles in the basic structure. In this work the influence of fluorine substitution of hydroxyl groups is examined. The powders of fluorine-substituted hydroxyapatite $Ca_{10}(PO_4)_6(OH)_{2-x}F_x$ (x = 1; 1.5; 2) were precipitated by chemical condensation from solutions. Such characteristics of powders as phase composition, morphology, particle size distribution, density, specific surface area have been studied. It was established that partial replacement of hydroxyl groups by fluorine leads to a decrease in the particle size to 10 nm. The degree of substitution affects the mechanical properties of synthesized powders and ceramics after annealing. A comparison of the particle size distribution in the initial samples and the distribution of grains in the sintered ceramics confirmed that the ceramics inherits the structure of the powders, which has a positive effect on its strength characteristics.

Keywords Hydroxyapatite · Fluorapatite · Nanopowders · Bioactive ceramics

1 Introduction

Dense or porous ceramics based on hydroxyapatite (HAP) is used as an implant material in many fields of medicine [1, 2]. The disadvantage of HAP-based bioceramics is a low mechanical strength, which limits its use for the elimination of defects in bone tissues experiencing regular and significant mechanical stresses [3]. A better durability can be achieved by transition to nanostructured materials, since ceramics based on such powders is characterized by a homogeneous structure, a near-zero open porosity, a small crystal size and increased strength [4, 5]. The small particle size and narrow size distribution of the initial powder aggregates suggest that it is possible to obtain ceramics with a homogeneous fine crystalline structure [6].

The fact that ceramics inherits the structure in the next technological stage indicates the importance of the production method, which determines the quality of the initial powder and, consequently, the microstructure and properties of final ceramics [6, 7]. In this regard, the "wet" methods of HAP synthesis, in particular, chemical condensation or precipitation from solutions, are of great interest, since they allow one to obtain powders with a high degree of dispersion and a well-developed surface and

provide a predetermined phase composition of ceramics after annealing [3, 6]. The wet methods are also more convenient for obtaining a homogeneous polycrystalline microstructure, since they exclude particle size growth, specific surface area reduction and crystal lattice imperfection occurring during solid-phase reactions [3, 6].

The degree of dispersion can be also increased by chemical modification of the structure of HAP during preparation of the initial powder. In this case, the introduction of fluorine ions into the structure is of interest. Such anionic substitution allows one to reduce the crystal lattice parameters and, as a result, to get a more nanostructured material, which will make it possible to obtain bioceramics exhibiting high hardness, strength and resistance to high temperatures and aggressive media.

Thus, the purpose of this work was to study the relationship between the composition, preparation method, microstructure and the mechanical properties of fluorine-substituted hydroxyapatite obtained by precipitation from solutions, as well as to estimate the influence of anion substitution on the microstructure and properties of the final ceramics.

2 Experimental methods

The samples of fluorohydroxyapatite $Ca_{10}(PO_4)_6(OH)_{2-x}F_x$ (x = 1; 1.5; 2) for studies were obtained by chemical condensation or precipitation from solutions [8]. The stoichiometric HAP, taken as a reference specimen, was also obtained by precipitation from solutions [9].

The X-ray diffraction analysis (XRD) was performed on Shimadzu and DRON-2.0 diffractometers in CuKα radiation with the angle interval $10° \leq 2\Theta \leq 70°$, a scanning step of 0.03° and 2 s time in point. The phases were identified with the use of the Powder Diffraction File JCPDSD-ICDD PDF2 (sets 1–47). The composition of the obtained samples was also confirmed by energy-dispersive X-ray analysis on a JSM 6390 LA, JEOL microscope with an energy-dispersion X-ray analyzer EX-23010BU (the quantitative error of the analyzer is 1% at cathode voltage of 20 kV and focal spot size of 60 nm). Some examples of typical XRD and EDX patterns are presented in the Supplementary.

The tablets were formed from 0.5 to 1.0 g powder samples by uniaxial two-sided pressing without bundle in a cylindrical steel mold with a diameter of 10 mm on a hydraulic hand press at room temperature and pressure 20 MPa.

The samples were annealed in a Nabertherm L 9/11 muffle furnace in air in the temperature range 200–1000 °C with a step of 200 °C at a heating rate of 10 °C/min with the exposure time of 1 h and cooled to room temperature with the furnace.

The specific surface area was determined by the Brunauer–Emmett–Taylor (BET) method of low-temperature nitrogen adsorption on a Gemini VII 2390 V1.03 (V1.03 t) automatic surface and porosity analyzer (Micromeritics). The samples were preliminarily degased at T = 200 °C for 1 h on a VacPrep 061 Sample Degas System (Micromeritics).

The density was measured with a helium pycnometer AccuPyc II 1340 (Micromeritics) at room temperature. The pycnometer cell (1 cm³) was filled by 50–60% with the test material and 15 measurements were performed for each sample.

Based on the results of the measurements, the size of powder particle (the average surface diameter D, nm) was evaluated in the spherical approximation by the formula [5]:

$$D = 6000/S_s \cdot \rho, \tag{1}$$

where S_s is the specific surface area, m²/g and ρ is the density, g/cm³.

The surface of the samples was studied by high resolution raster electron microscopy (REM) using an Ultra 55 Carl Zeiss microscope (magnification from × 12 to × 900,000, resolution of 1.0 nm at 15 kV) and by scanning electron microscopy (SEM) on a JSM 6390 LA, JEOL microscope (magnification from × 5 to × 300,000, resolution of 3.0 nm at 30 kV).

The particle size was determined on a universal particle size distribution laser express analyzer Horiba LA-950 in the measurement range from 0.01 to 3000 µm with the maximum error 0.6%. The refraction coefficients are 1.644–1.65 and 1.631–1.65 for HAP and FAP, respectively.

The microhardness of the samples was measured by the Vickers method on a PMT-3M microhardness tester with a load of 0.98 N (100 g) and loading time 10 s. For each composition, 10 measurements were carried out. The values of microhardness (HV, hardness units) were calculated by the formula:

$$HV = 0.189P/d^2 \cdot 10^6, \tag{2}$$

where P is the normal load applied to the diamond tip, N, and d is the arithmetic average of the lengths of both diagonals of the imprint, µm.

3 Results and discussion

According to the XRD data, the synthesized powders represent a weakly crystallized apatite phase, as evidenced by wide weak diffraction peaks. With a rise in the annealing temperature, the degree of crystallinity of all samples increased. The more pronounced diffraction peaks of

smaller width and the separation of the doublets point to better crystallization of the material and a higher degree of long-range order.

The morphology of the crystals depends on the composition of the sample and the sintering temperature (Fig. 1). REM analysis of the morphology of the initial samples indicates the presence of primary aggregates consisting of particles of submicron size 50–100 nm. The well developed surface of the initial powders is due to the small contact area of the particles and the presence of pores. It is seen that the specific surface area increases with the content of fluorine ions (Table 1).

Owing to the submicron particle size, the powders obtained by chemical condensation have a large surface energy, which tends to decrease during spontaneous aggregation both at the synthesis and ceramic production stages [7], which explains the enlargement of particles for the samples annealed at 800 °C.

The morphological features of the samples at 800 °C are oriented packing of grains, formation of bridges between individual elements of the microstructure and channel pores, indicating liquid-phase sintering processes. The structure represents sintered particles of 100–400 nm size (Fig. 1). It should be noted that the
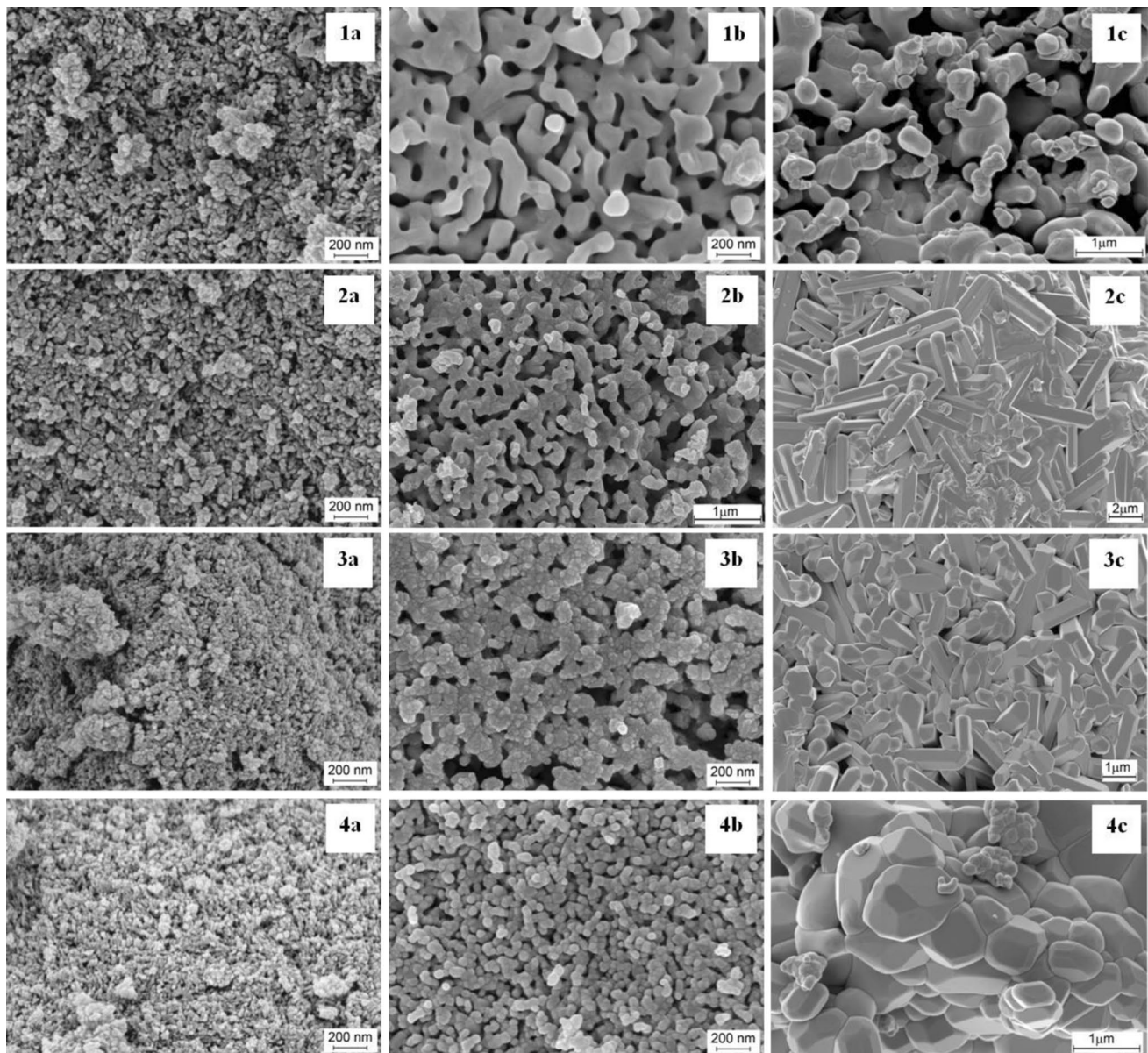

Fig. 1 REM images of samples annealed at different temperatures: 1-$Ca_{10}(PO_4)_6(OH)_2$: 2-$Ca_{10}(PO_4)_6(OH)F$; 3-$Ca_{10}(PO_4)_6(OH)_{0.5}F_{1.5}$; 4-$Ca_{10}(PO_4)_6F_2$, a-25 °C; b-800 °C; c-1000 °C

Table 1 The results of measurements of specific surface area and porosity of samples

Sample	Specific surface area (m^2/g)		
	25 °C	800 °C	1000 °C
$Ca_{10}(PO_4)_6(OH)_2$	98.8021 ± 0.6497	12.1472 ± 0.1236	0.4359 ± 0.0126
$Ca_{10}(PO_4)_6(OH)F$	97.5297 ± 0.5123	9.3687 ± 0,0743	0.2003 ± 0.0072
$Ca_{10}(PO_4)_6(OH)_{0.5}F_{1.5}$	131.8210 ± 0.7997	15.1587 ± 0.0495	0.3666 ± 0.0143
$Ca_{10}(PO_4)_6F_2$	144.7631 ± 0.8499	24.4146 ± 0.1435	1.4805 ± 0.0126
Pore area (m^2/g)			
$Ca_{10}(PO_4)_6(OH)_2$	10.3677	0.7829	0.3455
$Ca_{10}(PO_4)_6(OH)F$	5.7738	0.6915	0.0468
$Ca_{10}(PO_4)_6(OH)_{0.5}F_{1.5}$	9.2536	–	0.2043
$Ca_{10}(PO_4)_6F_2$	10.3005	2.54975	–
Pore volume (cm^3/g)			
$Ca_{10}(PO_4)_6(OH)_2$	0.005483	0.000474	0.000197
$Ca_{10}(PO_4)_6(OH)F$	0.002746	0.000367	0.000032
$Ca_{10}(PO_4)_6(OH)_{0.5}F_{1.5}$	0.004657	–	0.000126
$Ca_{10}(PO_4)_6F_2$	0.005141	0.001311	–

grain size decreases as the degree of substitution in the HAP structure increases. Thus, the ceramics inherits the nanopowder structure due to the introduction of fluorine ions.

After annealing at 1000 °C, the total porosity of all samples decreases, the number of individual closed pores increases and the ratio of channel pores lowers. For fluorine-substituted HAP, the convergence of particle centers is typical, their contact area increases, and the crystallization of secondary columnar crystals with a clear hexagonal facet is observed, which leads to the consolidation of ceramics [10].

The sintering process is accompanied by an increase in the particle size, and the grain size depends on the degree of substitution: the $Ca_{10}(PO_4)_6(OH)F$ sample has a crystal size of ~ 5–10 μm, $Ca_{10}(PO_4)_6(OH)_{0.5}F_{1.5}$—~ 1–5 μm, and $Ca_{10}(PO_4)_6F_2$—~ 0.5–1 μm.

The morphology of the samples annealed at 1000 °C (Fig. 1) indicates that the rate of secondary recrystallization processes increases with the concentration of fluorine ions, i.e. with reduction of the size of initial crystallites in the sample.

The morphological data obtained by the REM method are consistent with the values of the mean surface diameter of particles calculated from the specific surface area

(Table 1) and pycnometric density data (Table 2) and also correlate with the results of dispersion analysis (Fig. 2).

It was found with the use of the laser diffraction method that both initial and annealed powder samples have a rather wide particle size distribution (Table 3). The particle size distribution histograms for the initial powders are typical unimodal curves showing a similar distribution pattern for all samples (Fig. 2a). The asymmetry of the curves can be explained by spontaneous aggregation of submicron particles, which is characteristic of powders obtained by precipitation from solutions. The maximum size of the aggregates of the initial powder materials did not exceed 12 μm. The average particle sizes determined by the laser diffraction method are given in Table 4. Note that the nature of the particle distribution in powders and grains of ceramics sintered at 800 °C is similar (Fig. 2b). The maximum aggregate size in this case did not exceed 14 μm. According to the histograms, an increase in the fluorine ion content in the HAP structure promotes a more homogeneous particle size distribution.

For $Ca_{10}(PO_4)_6F_2$, the maximum on the powder particle size distribution curve corresponds to the maximum on the grain size distribution curve in the ceramic structure at 800 °C (Fig. 2, Table 4), i.e. the grain size of $Ca_{10}(PO_4)_6F_2$ based ceramics is actually determined by the size of

Table 2 Pycnometric density of samples

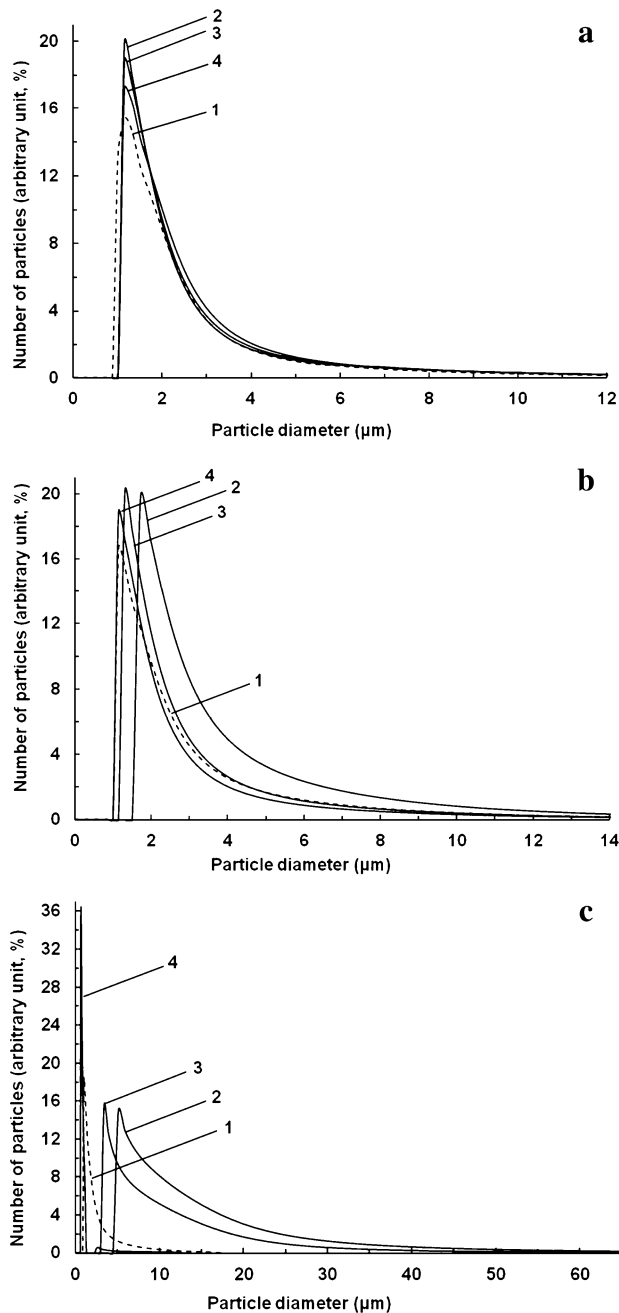| Sample	Density, ρ (g/cm^3)		
	25 °C	800 °C	1000 °C
$Ca_{10}(PO_4)_6(OH)_2$	2.9293 ± 0.0009	3.0827 ± 0.0017	3.1477 ± 0.0075
$Ca_{10}(PO_4)_6(OH)F$	2.8370 ± 0.0010	3.0923 ± 0.0012	3.0699 ± 0.0007
$Ca_{10}(PO_4)_6(OH)_{0.5}F_{1.5}$	2.8854 ± 0.0010	3.0963 ± 0.0021	3.0620 ± 0.0006
$Ca_{10}(PO_4)_6F_2$	1.8876 ± 0.0013	3.0888 ± 0.0014	3.0919 ± 0.0016

Fig. 2 The particle size distribution in powder samples at different temperatures: 1-$Ca_{10}(PO_4)_6(OH)_2$; 2-$Ca_{10}(PO_4)_6(OH)F$; 3-$Ca_{10}(PO_4)_6(OH)_{0.5}F_{1.5}$; 4-$Ca_{10}(PO_4)_6F_2$, **a** 25 °C; **b** 800 °C; **c** 1000 °C

Table 3 Mathematical estimation of particle sizes

Sample	Medium surface diameter, D (nm)		
	25 °C	800 °C	1000 °C
$Ca_{10}(PO_4)_6(OH)_2$	20.73	160.22	4361.91
$Ca_{10}(PO_4)_6(OH)F$	21.68	207.10	9772.31
$Ca_{10}(PO_4)_6(OH)_{0.5}F_{1.5}$	15.77	127.83	5339.25
$Ca_{10}(PO_4)_6F_2$	21.96	79.56	1310.30

Table 4 The results of dispersion analysis of samples

Sample	Average particle size (μm)		
	25 °C	800 °C	1000 °C
$Ca_{10}(PO_4)_6(OH)_2$	1.78	2.09	1.82
$Ca_{10}(PO_4)_6(OH)F$	1.88	2.92	10.33
$Ca_{10}(PO_4)_6(OH)_{0.5}F_{1.5}$	1.89	2.18	7.33
$Ca_{10}(PO_4)_6F_2$	1.96	1.94	0.87

primary aggregates, which confirms that for this sample the ceramics inherits the structure of initial powder.

The $Ca_{10}(PO_4)_6(OH)F$ and $Ca_{10}(PO_4)_6(OH)_{0.5}F_{1.5}$ samples annealed at 1000 °C are characterized by the asymmetrical unimodal curves with "tails" extended into the region of large dimensions, which indicates a considerable aggregation of primary particles (Fig. 2c). The spread of the values is 5–70 μm for $Ca_{10}(PO_4)_6(OH)F$ and 3–59 μm for $Ca_{10}(PO_4)_6(OH)_{0.5}F_{1.5}$.

The analysis of the distribution curves at 1000 °C suggests that the rate of the recrystallization processes increases with the growth of the fluorine content in the HAP structure. Thus, the appearance of secondary aggregates (~ 2% of the total number of particles) is observed at this temperature for the composition $Ca_{10}(PO_4)_6F_2$, as evidenced by the characteristic bimodal distribution with two maxima corresponding to primary aggregates (in the particle size range 0.7–1.2 μm) and secondary aggregates (in the range 3–12 μm).

According to the earlier studies [10], further temperature treatment of $Ca_{10}(PO_4)_6F_2$, leads to a shift of the particle size into the region of large values and to the predominance of secondary aggregates (Fig. 3). The grains in the sintered ceramics at 1300 °C do not contain intracrystalline porosity because the pores are removed from the material before the recrystallization begins. According to the literature data [6, 11], the time gap between the compaction and grain growth promotes the production of dense fine-grained ceramics.

The temperature dependence of microhardness (Fig. 4) for all $Ca_{10}(PO_4)_6(OH)_{2-x}F_x$ samples (x = 0; 1; 1.5; 2) has a minimum at 400 °C, associated with a variation in the crystal lattice ordering, which is due to the loss of lattice-adsorbed water and a certain amount of carbonate ions. With a rise in temperature to 800 °C, the substance crystallizes and the degree of crystallinity increases, which provides a monotonic enhancement of the microhardness.

The introduction of fluorine ions into the structure of HAP makes it possible to increase the strength characteristics approximately three times. The microhardness of the samples increases proportionally with the degree of anionic substitution in the structure. The higher durability in this case is explained by the smaller size of identical
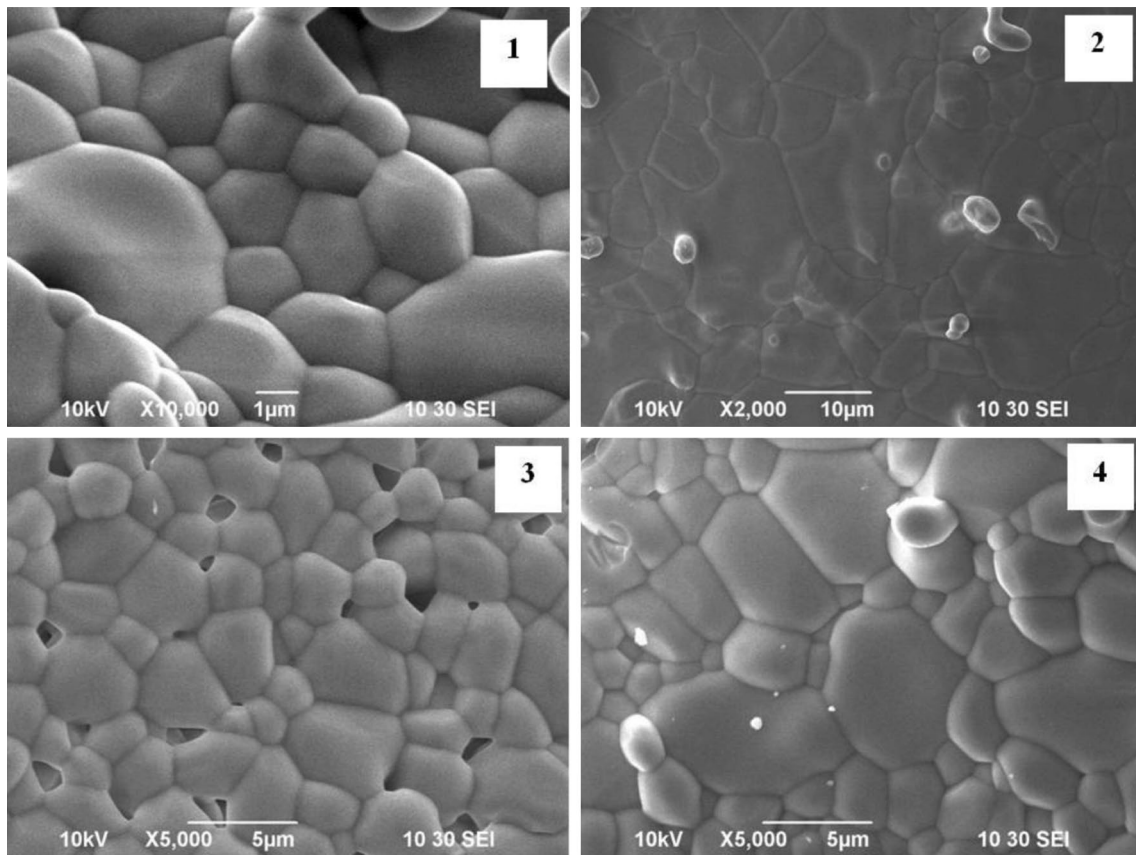
Fig. 3 SEM images of the samples annealed at 1300 °C: 1-$Ca_{10}(PO_4)_6(OH)_2$; 2-$Ca_{10}(PO_4)_6(OH)F$; 3-$Ca_{10}(PO_4)_6(OH)_{0.5}F_{1.5}$; 4-$Ca_{10}(PO_4)_6F_2$

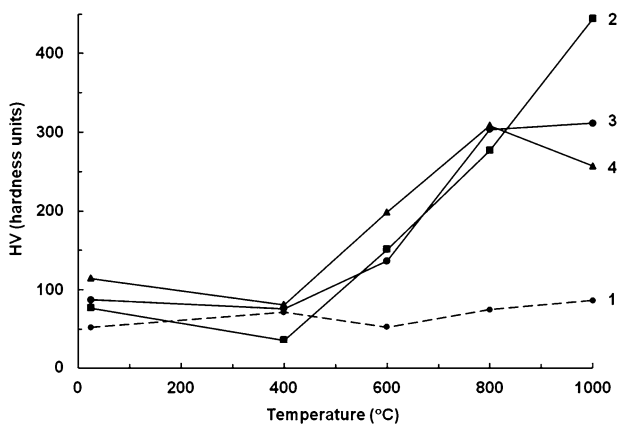**Fig. 4** The microhardness of the samples as a function of the sintering temperature: 1-$Ca_{10}(PO_4)_6(OH)_2$; 2-$Ca_{10}(PO_4)_6(OH)F$; 3-$Ca_{10}(PO_4)_6(OH)_{0.5}F_{1.5}$; 4-$Ca_{10}(PO_4)_6F_2$

crystals composing the substance. The microhardness as a function of temperature has a maximum at 800 °C. The fact that the ceramics inherits the nanopowder structure characteristic of $Ca_{10}(PO_4)_6F_2$ provides better strength characteristics at this annealing temperature. The subsequent decrease in the microhardness at 1000 °C is a result of collective recrystallization and coarsening of grains and is the more pronounced, the higher is the content of fluorine ions in the HAP structure.

4 Conclusions

As a result of the research it was established that anionic substitution in the structure of HAP has a significant impact on the microstructure and strength properties. The introduction of fluorine ions into the structure of HAP allows the microhardness of the material to be significantly increased.

It is shown that heat treatment at 800 °C of the nanopowders synthesized from $Ca_{10}(PO_4)_6(OH)_{2-x}F_x$ solutions (x = 1; 1.5; 2) leads to their coarsening, with the nanodimensional particle size being preserved, and that the ceramic samples obtained on their basis consist of smaller crystals and possess greater strength, in agreement with the known data [4, 5].

$Ca_{10}(PO_4)_6F_2$ exhibits the maximal strength characteristics among the examined samples in the temperature

range 25–800 °C. During subsequent annealing at 1000 °C, an opposite effect of the anion substitution degree on the strength characteristics is observed: the microhardness decreases when the degree of substitution by fluorine ions increases. The decrease in the microhardness is due to the heterogeneity characteristic of secondary recrystallization.

Thus, the fluorine-substituted HAP $Ca_{10}(PO_4)_6(OH)_{2-x}F_x$ (x = 1; 1.5; 2) meets the requirements for powder materials suitable for the preparation of ceramics. The dependence of the microhardness of fluorine-substituted HAP on the phase composition of the sample and the annealing temperature will allow one to vary the temperature regimes for obtaining ceramic materials with specified properties.

Availability of data and material Data and materials described in the manuscript will be freely available to science community for non-commercial use.

Compliance with ethical standards

Conflict of interest On behalf of all authors, the corresponding author states that there is no conflict of interest.

References

1. Kantharia N, Naik S, Apte S, Kheur M, Kheur S, Kale B (2014) Nano-hydroxyapatite and its contemporary applications. J Dent Res Sci Dev 1(1):15–19
2. Putlyaev VI, Safronova TV (2006) A new generation of calcium phosphate biomaterials: the role of phase and chemical compositions. Glass Ceram 63(3–4):99–102
3. Zhang Y, Lu J, Yang S (2012) Preparation of hydroxyapatite ceramic through centrifugal casting process using ultra-fine spherical particles as precursor and its decomposition at high temperatures. J Adv Ceram 1(1):60–65
4. Bakunova NV, Komlev VS, Shvorneva LI, Fedotov AYu, Fomin AS, Barinov SM, Ievlev VM, Ponomarev YuA, Soldatenko SA (2011) Effect of thermal processing on characteristics of nanopowders of hydroxyapatite. Inorg Mater Appl Res 2(1):25–30
5. Petrakova NV, Barinov SM, Evstratov EV, Alymov MI, Ashmarin AA, Shvorneva LI, Egorov AA, Kutsev SV (2017) Compaction of hydroxyapatite nanopowders by hydrostatic pressing. Inorg Mater Appl Res 8(4):528–534
6. Safronova TV, Shekhirev MA, Putlyaev VI, Tretyakov YuD (2007) Densification additives for hydroxyapatite ceramics. Inorg Mater 43(8):901–909
7. Belyakov AV, Bakunov VS (2006) Structural evolution in ceramic technology and processing. Refract Ind Ceram 47(1):48–52
8. Bogdanova EA, Skachkov VM, Sabirzyanov NA (2018) Method of preparing apatite suspension. Pat. RU 2652193. Bull. 12
9. Sabirzyanov NA, Bogdanova EA, Khonina TG (2010) Method of preparing hydroxyapatite suspension. Pat. RU 2406693. Bull. 35
10. Barinov SM (2010) Calcium phosphate-based ceramic and composite materials for medicine. Russ Chem Rev 79(1):13–29
11. Putlayev V, Veresov A, Pulkin M et al (2006) Silicon-substituted hydroxyapatite ceramics (Si-HAp): densification and grain growth through the prism of sintering theories. Materialwiss Werkst 37(6):416–421